



# Two dimensional modelling of the interaction between electromagnetic waves and plasma-metamaterial composite structures using the particle-in-cell method

D. Tsiklauri \* and I. Morrison 

*Joule Physics Laboratory, School of Science, Engineering and Environment,  
University of Salford, Manchester, M5 4WT, United Kingdom*

(Dated: June 12, 2025)

In this work we (i) extend previous 1D studies of electromagnetic (EM) wave propagation in an over-dense plasma-metamaterial composite into two spatial dimensions and (ii) study blocking of EM waves by the composite 2D structures (barriers). Such barriers are formed when metamaterial spatially co-exists with a plasma density depletion in a form of a slab or two-dimensional density rectangular depletions (DRDs). This is analogous to EM wave trapping by preformed density cavities in near-critical density plasmas, studied before. We find that plasma-metamaterial composite allows to block EM waves by both slab and DRD configurations, thus forming a standing wave at the edge of an opaque region. The standing wave subsequently damps which offers applications such as heat deposition or substrate materials (micro)machining depending on EM wave intensity. The established results may find future applications such as: more efficient plasma vapour deposition, controlling EM wave propagation (EM wave blocking) in invisibility cloaks and alike. The EM wave blocking conditions are elucidated by a set of particle-in-cell (PIC) numerical simulations.

## I. INTRODUCTION

Ref. [1] gives a good background and lays a foundation to the considered research. It is well-known that industrial applications such as physical vapor deposition (PVD), material surface treatment and many others use plasma as an agent or a means of delivery [2]. This technology bridges the gap between conventional thermal spray and vapor deposition and provides a variety of coating microstructures composed of vapor, liquid, and solid deposition units.

A common method of creation of plasma in these applications is gas irradiation by microwaves. Microwaves are a form of electromagnetic radiation with frequency range between 1 and 100 GHz (wavelengths between 300 and 3 mm). When a microwave enters a vessel with the plasma discharge, and the electron density  $n_e$  is larger than the cut-off density for the incident microwave, the latter cannot propagate through plasma and is confined to its surface [3]. In microwaves, the surface wave, with a typical width of electron inertial length  $c/\omega_{pe}$ , sustains the over-dense plasma, but the width of the generated plasma is narrow. Here the term over-dense plasma has the following meaning: Plasma is only transparent to EM wave with a frequency  $\omega_0$  larger than the electron plasma frequency  $\omega_{pe} = \sqrt{n_e e^2 / (m_e \epsilon_0)}$ , where  $n_e$  is the electron number density. In such case permittivity  $\epsilon_p = 1 - \omega_{pe}^2 / \omega_0^2$  is a positive, real number. In the opposite case when  $\omega_0 < \omega_{pe}$  the permittivity  $\epsilon_p$  becomes negative and plasma is opaque to such EM wave. In order to increase penetration of microwaves into the over-dense plasma, DC magnets or magnetic field coils are used. The magnetized plasma has the propagation band under the electron cyclotron frequency, and this enables to optimize this frequency by the strength of the external magnetic field. This propagation mode is the whistler mode, and a wavenumber becomes infinity when the incident wave frequency approaches the electron cyclotron frequency. The electron cyclotron reso-

nance (ECR) heating is useful for the efficient power injection into the overdense plasma, but it is difficult to prepare a large-scale DC magnet for the plasma generation systems. Metamaterials are artificial composites made of unit patterns whose size is much smaller than the wavelength of the corresponding waves. Metamaterials give the extraordinary propagation of EM waves and it cannot occur in natural materials. Refractive index  $N$  becomes negative in metamaterials because both permittivity  $\epsilon$  and permeability  $\mu$  become negative [4]. The experimental verification was performed with the combination of the split-ring resonators (SRRs) as negative- $\mu$  metamaterials [5]. Theoretical and numerical simulation studies of wave propagation in negative  $N$  are numerous [6–8].

Refs. [8, 9] reported the generation of the second harmonic waves in negative  $N$  with quadratic nonlinear response. Also the nonlinear frequency conversion process was demonstrated to be analogous to non-linear optics [10]. Also, experimental studies were performed with the combination of the arrays of metal wires as a negative- $\epsilon$  material [11–13]. The array of metal wires has a cut-off frequency and acquires negative  $\epsilon$  under the cut-off frequency as in the over-dense plasma [14]. A composite of an overdense plasma and a negative- $\mu$  metamaterial has been investigated experimentally [15–17] and by means of numerical simulations [18, 19]. It was demonstrated that that refractive index  $N$  was negative, the second harmonic wave was present in Ref. [16], and SRRs were electrically connected with plasma at a microscopic level [17], wave propagation was not clearly confirmed in the composite of an overdense plasma and a negative- $\mu$  metamaterial. Ref.[1] conducted 1D electromagnetic PIC simulations of EM wave propagation in the composite of overdense plasma and the negative- $\mu$  metamaterial. In their simulation EM waves enter the plasma-metamaterial composite, and propagate in it with a negative phase velocity and a positive group velocity. This way, Ref.[1] confirmed that the plasma-metamaterial composite has a negative refractive index. Ref. [20] gives an up-to-date background to the experimental implementation of the considered research. In particular Iwai *et al.* [20] conducted measurements of properties of transmitted microwaves

\* D.Tsiklauri@salford.ac.uk

and plasma parameters in a composite of double-split-ring resonators (DSRRs), which make magnetic permeability negative. In their experiments plasma was created using a 2.45 GHz microwave. They launched the microwaves with power in the range of 100 – 200 W, modulated by a pulse wave at a low frequency and a low duty ratio to detect time evolutions of plasma parameters. This way, Iwai *et al.* [20] performed the measurements at different positions with varying distance from the supporting plate of the DSRRs, and established the enhanced wave transmission in the composite with non-uniform profiles of electron temperature. They confirmed that the non-uniformity is due to the magnetic resonant behaviour of the DSRRs at the microscopic level, while their macroscopic manifestation is making the permeability negative, enhancing wave energy transfer inside the composite.

Ref.[18] performed FDTD simulations and reported the wave propagation with a negative  $N$  in the array of plasma columns under a negative- $\mu$  state. They assume that a propagating microwave contributes to simultaneous plasma generation by its electric field  $E$  that deforms  $\varepsilon$  and refractive index  $N$  in the metamaterial; this is a field-dependent metamaterial, in which a propagating wave conversely suffers from the changes of  $\varepsilon$  and/or  $N$ , where  $E$ ,  $\varepsilon$ , and  $N$  settle self-consistently. Such a metamaterial may exhibit nonlinear features due to its field-dependent properties. Ref.[19] studied the local electromagnetic fields around an SRR when a plasma exists near the SRR. Since both reports used the FDTD solver to simulate EM wave coupling to plasmas i.e. coupling between high-frequency EM waves and the plasma occurs mainly via the electron current density (ions are heavy enough not to respond in EM field variations). Hence in both Ref.[18] and Ref.[19] the kinetic effects such as self-consistent EM fields from collection of billions of particles in plasma were not considered. These effects must be included in the case when a high-power electromagnetic wave enters the overdense plasma under a negative- $\mu$  state.

Although, Ref.[1] conducted fully kinetic electromagnetic PIC simulations of EM wave propagation in the composite of overdense plasma and the negative- $\mu$  metamaterial, they used PIC code modified from KEMPO1 which is *spatially 1 dimensional (1D)*. There is a clear need to extend model of Ref. [1] beyond simple 1D case. This has very strong industrial applications in plasma processing. i.e. use of negative- $\mu$  metamaterial (the plasma-metamaterial composite) will enable to increase plasma density which is crucial for plasma processing efficiency. It can be also related to modern applications such as ion thrusters and plasma based acceleration, intense X-Ray sources etc. Typical microwaves used today have frequencies in the few GHz range and the cut-off density that corresponds to the cut-off frequency  $f_{pe} = \omega_{pe}/2\pi$  is few  $10^{16} \text{ m}^{-3}$ . If this density can be increased then plasma processing will become more efficient, as the reaction rate is usually proportional to the product of number densities of the reactant species. Thus, in this work propose to extend previous 1D results [1] into two spatial dimensions and use the modified 2D (and in the future 3D) EPOCH PIC code [21]. The key novelty is that we propose to use much more general, fully kinetic regime using EPOCH code, while all previous research [18, 19] used FDTD

method to simulate plasmas, hence kinetic effects of a plasma and non-linearity were not considered. These effects must be included when a high-power EM wave enters the overdense plasma under a negative- $\mu$  state.

The second input and motivation for the present study comes from research related to the trapping of EM waves in preformed density cavities in near-critical density plasmas [22–26]. In a more broader context, the present research is about an ability to control and manipulate EM radiation by means of combining the presence of plasma and metamaterials. In particular Ref. [26] studied EM wave trapping in cavities in near-critical density plasmas using 2D particle-in-cell (PIC) simulation. They find that in plasma, laser’s ponderomotive force can create a vacuum cavity bounded by a thin overcritical-density wall. The EM waves are self-consistently trapped as a half-cycle electromagnetic wave in the form of an oscillon-caviton structure. Further, the trapped EM wave is slowly depleted through interaction with the cavity wall. Ref. [26] also studied a situation when a near-critical density plasma contains a *preformed* density cavity and found that EM wave becomes trapped, forming a standing wave. They find that the trapped light is characterized as multi-peak structure and that the overdense plasma layer formed around the self-generated and preformed cavities that is induced by the laser ponderomotive force is the natural reason for EM wave trapping. Ref. [26] also discusses possible applications of the EM wave trapping in preformed and self-consistently generated by EM wave’s ponderomotive force density cavities in near-critical density plasmas.

We close the introduction by stating the aims of this work that are two-fold: (i) to extend previous one dimensional studies of electromagnetic (EM) wave propagation on an overdense plasma-metamaterial [1] composite into two spatial dimensions and (ii) to study blocking of EM waves by the composite barriers in analogy with their trapping in preformed density cavities in near-critical density plasmas [26]. We therefore propose to use modified 2D EPOCH code, as described in section 2.

## II. THE MODEL

We modify the existing state-of-the-art, fully kinetic, explicit, electromagnetic, 2D, particle-in-cell (PIC) code called EPOCH [21]. The modification is by adding the effect of negative- $\mu$  metamaterial (the plasma-metamaterial composite) via adding the magnetic current term,  $\mathbf{J}_m$ , to the relevant Maxwell’s equation as following:

$$\nabla \times \mathbf{E} = -\mathbf{J}_m - \frac{\partial \mathbf{B}}{\partial t}, \quad (1)$$

$$\frac{\partial \mathbf{J}_m}{\partial t} = \omega_m^2 \mathbf{B}, \quad (2)$$

where  $\omega_m$  is the magnetic resonance frequency. It does not have any associated mathematical expression like the electron plasma frequency has  $\omega_{pe} = \sqrt{n_e e^2 / (m_e \epsilon_0)}$ .  $\omega_m$  is just a constant that quantifies the effect of presence metamaterial

in the numerical simulation. In the experiments such as Iwai *et al.* [20]  $\omega_m$  is prescribed by the material properties and physical dimensions of DSRRs. The modification of EPOCH code is insertion of  $\mathbf{J}_m$ . The metamaterial effect, based on  $\mathbf{J}_m$ , does not affect both electric field,  $\mathbf{E}$ , and plasma in this simulation.  $\mathbf{J}_m$  is determined only by  $\mathbf{B}$  and the constant value of  $\omega_m$ . According to Ref.[1] such approach has proven to be very effective in modeling of bulk effects of negative- $\mu$  metamaterial. We would remark that to model the response of a magnetic negative (MNG) material we also use, as in [1], the Drude model, and as for the response of the epsilon negative (ENG) permittivity of plasma. However, MNG materials are usually obtained using resonant substructures such as split-ring resonators (SRR) which are generally not accurately modeled with the Drude model. In particular, perhaps some other, a more accurate model, is needed to better describe the narrow band behavior of the MNG material in the PIC simulation. This can be a subject to future investigation. The plane, linearly-polarized EM wave is excited by the external current  $\mathbf{J}_s$  at  $x = 1\Delta$ , the first grid point of the simulation domain, where  $\Delta = r_D = \sqrt{\epsilon_0 k_B T_e / (n_e q_e^2)}$  is the Debye length.  $\mathbf{J}_s$  oscillates in vertical  $z$ -direction  $\mathbf{J}_s = \hat{z} J_z = J_0 \sin(\omega_0 t)$ . EM wave travels in  $x$ -direction and has components  $E_z$  and  $B_y$  as it travels initially in free-space. The plasma-metamaterial composite exists in the region where  $12.8 < x < 25.6$ , see Figure 2(a), that we call *plasma region*. The sketch of the numerical simulation is very similar to Fig.1 from Iwai *et al.* [1], so it is not duplicated here. Note that spatial dimensions are normalized by the EM wave inertial length  $c/\omega_0$ . When EM wave enters the plasma region it excites a different current  $\mathbf{J}_p$  (subscript p stands for plasma), which is prescribed by the following equations:

$$\nabla \times \mathbf{B} = \mu_0 \mathbf{J}_p + \mu_0 \epsilon_0 \frac{\partial \mathbf{E}}{\partial t}, \quad (3)$$

$$\frac{d(\gamma v_\alpha)}{dt} = \frac{q_\alpha}{m_\alpha} (\mathbf{E} + \mathbf{v}_\alpha \times \mathbf{B}), \quad (4)$$

where  $\mathbf{J}_p$  in equation (3) is different from the initial  $\mathbf{J}_s$  because when EM wave enters plasma-metamaterial composite, electrons and ions start to oscillate and  $\mathbf{J}_p$  is now prescribed by dielectric response of plasma and velocity of oscillating plasma particles of species  $\alpha$ ,  $\mathbf{v}_\alpha$ . EPOCH is a relativistic code therefore, note that in Eq.(4),  $\gamma$  is the Lorentz  $\gamma$ -factor. In our case it is very close to unity. Note that when EM wave amplitude and/or plasma number density are small, plasma has the simple dispersive back-reaction to EM wave's  $\mathbf{E}$  as  $\partial \mathbf{J}_p / \partial t \approx \omega_{pe}^2 \mathbf{E}$  where  $\omega_{pe}$  is the plasma frequency. When metamaterial is present its effect is felt by resonant interaction of EM wave's magnetic field  $\mathbf{B}$ . The effect of magnetic resonance can be described by appearance of another frequency  $\omega_m$ , which appears in equation (2). Note that in equation (2), the term  $\partial \mathbf{J}_m / \partial t = \omega_m^2 \mathbf{B}$  is mathematically similar to  $\partial \mathbf{J}_p / \partial t \approx \omega_{pe}^2 \mathbf{E}$ . This effectively means that presence of metamaterial is manifest by additional current  $\mathbf{J}_m$ . In this formulation, the metamaterial does not affect  $\mathbf{E}$  and plasma in this simulation.  $\mathbf{J}_m$  is determined only by  $\mathbf{B}$  and the constant

$\omega_m$ . Note that plasma current  $\mathbf{J}_p$  is prescribed by nonlinear and kinetic motions of the particles and consists of the  $x$ - and  $z$ -axis components. The magnetic current density  $\mathbf{J}_m$  is parallel to  $\mathbf{B}$  and consists of the  $y$ -axis component. Therefore effective permittivity of the plasma  $\epsilon_p$  and the effective permeability of the metamaterial  $\mu_m$  are expressed as  $\epsilon_p = 1 - \omega_{pe}^2 / \omega_0^2$  and  $\mu_m = 1 - \omega_m^2 / \omega_0^2$ . This implies that is EM wave's frequency  $\omega_0$  is smaller than both  $\omega_{pe}$  and  $\omega_m$  ( $\omega_0 < \omega_{pe}$  and  $\omega_0 < \omega_m$ ) thus both  $\epsilon_p$  and  $\mu_m$  are negative. Therefore, refractive index  $N = \sqrt{\epsilon_p \mu_m} = i^2 \sqrt{|\epsilon_p| |\mu_m|} = -\sqrt{|\epsilon_p| |\mu_m|}$  becomes negative with all of the above described consequences such a EM wave's negative phase speed propagation in an over-dense plasma-metamaterial composite region [1].

The numerical recipe how to add the additional term responsible for the presence of the metamaterials is given in appendix A. Here we focus on the details of the numerical simulation set up. We use periodic boundary conditions, both in  $x$ - and  $y$ -directions, throughout this work, which numerically are the most precise of all available boundary conditions. In order to avoid the spurious reflections, and to conserve the total energy in the simulation, we do not to use open or absorbing boundary conditions in EPOCH so that to remove the wave propagating towards negative  $x$  and thus reduce the computational domain. Our choice of periodic boundary conditions means that the solution that is generated at  $x = 1\Delta$ , the first grid cell, that travels to the left, i.e. negative  $x$ -direction, and re-enters the simulation domain from the far right side of the domain  $x = x_{\max}$ , should not collide with the main studied numerical solution that travels in positive  $x$ -direction. This is achieved by the setting  $x = x_{\max} = 8192\Delta$ . It can be seen from Fig.1(a) that the left- and right- going numerical solutions never collide. The above defined notation for the Debye length can be also written as  $\Delta = \lambda_D = v_{th,e} / \omega_{pe} = \sqrt{k_B T_{e,max} / m_e} / \omega_{pe}$ . Maximal temperature is set as  $T_{e,max} = m_e (0.0375c)^2 / k_B$ . We use the term maximal temperature because it actually varies across  $x$ -axis. This is because as in Ref.[27] we keep pressure balance by making  $p_{e,i} = n_{e,i}(x) k T_{e,i}(x) = const$ , i.e.  $T_{e,i}(x) = T_{e,i,max} [n_0 / n_{e,i}(x)] \propto 1 / n_{e,i}(x)$ . This ensures that the total initial pressure balance  $p_{e,i} = const$  is fulfilled.  $n_0$  is the background plasma number density, which is the same both for electrons and protons. The proton to electron mass ratio is set to the realistic value of 1836. The number densities  $n_{e,i}$  and grid sizes are varied in different numerical runs as specified in Table I.

In EPOCH code physical quantities are in SI units, so we fix  $n_0 = 10^{15}$  particles per  $m^{-3}$  typical of many laboratory (and accidentally astrophysical plasmas too). In cases 1a or 1c electron and ion number densities are set to  $10^{-2} n_0$  particles per  $m^{-3}$ . The factor  $10^{-2}$ , while drops number density to nearly zero, stops EPOCH from slowing down for numerical reasons. So effectively the cases with the constant values of  $10^{-2} n_0$  or other spatial locations, when number density is varying, can be referred to as 'no plasma', i.e. effectively a vacuum.

We use 100 particles per cell for each species, so in total, in the large runs, we have  $2 \times 100 \times 8192 \times 128 = 2.1 \times 10^8$  particles. One numerical run takes circa 2 days, 4 hours and 20

TABLE I: Table of numerical runs considered. See text discussing Fig.3 for the explanation of the notation used.

Case	$n_{e,i}(x)$	Grid $n_x \times n_y$	Metamat.	F
1a	$10^{-2}n_0$	$8192 \times 3$	N	-
1b	Eq.(5)	$8192 \times 3$	N	-
1c	$10^{-2}n_0$	$8192 \times 3$	Y	-
1d	Eq.(5)	$8192 \times 3$	Y	-
2	Eq.(5)	$8192 \times 128$	Y	-
3	Eq.(7)	$8192 \times 128$	Y	0.20
4	Eq.(7)	$8192 \times 128$	Y	0.99
5	Eq.(8)	$8192 \times 128$	Y	0.20
6	Eq.(8)	$8192 \times 128$	Y	0.99

minutes on 8 processor cores of the 40-core Intel(R) Xeon(R) CPU E5-2630, 2.20GHz Linux server. We checked numerical convergence of the presented results. Twice coarser grid and twice less number of particles yields numerical results which look the same at plotting accuracy i.e. 1 %. The length is normalized on  $c/\omega_0$ . The end simulation time is set  $t_{\text{end}} = 100/\omega_0$ . Note that electron inertial length,  $c/\omega_{pe}$ , is resolved with 27 grid points, i.e.  $(c/\omega_{pe})/\Delta = 26.67$ , while "EM wave" inertial length (this is not an accepted terminology),  $c/\omega_0$ , is resolved with 40 grid points, i.e.  $(c/\omega_0)/\Delta = 40$ . This means that the numerical resolution used is appropriate to resolve the smallest relevant electron kinetic scales considered. In all our time-distance plots in figures 1-6 we use 500 time snapshots, which means that data is stored every  $\Delta t = 0.2/\omega_0$ . This ensures smoothness of the time-distance plots.

### III. THE RESULTS

In this section we present the results of our numerical simulations detailed in table I. Below we also provide the justification for the number density expressions used in this work.

The electron and ion number densities are set using EPOCH's conditional function called  $\text{if}(a, b, c)$ . If  $a$  condition is *true*, the function returns  $b$ , otherwise the function returns  $c$ . For example, in the case 1b or 1d we set electron and ion number densities using

$$n_{e,i}(x) = \begin{cases} \text{if } [(x < 512/n_x x_{\text{max}}) \\ \text{or } (x > 1024/n_x x_{\text{max}}), 10^{-2}n_0, n_0], \end{cases} \quad (5)$$

which means that this conditional function returns the following expression

$$n_{e,i} = \begin{cases} 10^{-2}n_0, & \text{if } (x < 512/n_x x_{\text{max}}) \text{ or } (x > 1024/n_x x_{\text{max}}) \\ n_0, & \text{otherwise.} \end{cases} \quad (6)$$

Here the grid points number 512 and 1024 in  $x$ -direction correspond to  $x = 12.8$  and  $x = 25.6$  respectively. Note EPOCH maths parser uses  $lt$  instead of  $<$  and  $gt$  instead of  $>$  signs, see EPOCH user manual section 3.19 for details. In cases 1b or 1d the number density (given by equation(5)) is similar to case 2 (figure 2(a)), but in case 1b or 1d has  $n_y = 3$ , while for case 2

we set  $n_y = 128$ . Number density at time zero is plotted in case 2 only (figure 2(a)). Essentially this is a slab of plasma with top hat density of  $n_0 = 10^{15} \text{ m}^{-3}$  between 512 and 1024 grid points in  $x$ -direction, while on domain edges number density drops to  $10^{-2}n_0$ . For the case 2 we use number density given by equation (5). For the cases 3 and 4 the number density used is given by equation (7)

$$n_{e,i}(x) = \begin{cases} \text{if } [(x < 512/n_x x_{\text{max}}) \\ \text{or } (x > 1024/n_x x_{\text{max}}), 10^{-2}n_0, n_0] \\ - F \times \text{if } [(x > 896/n_x x_{\text{max}}) \\ \text{or } (x < 640/n_x x_{\text{max}}), 0, n_0]. \end{cases} \quad (7)$$

This means that we subtract  $F \times n_0$  in the region between 640 and 896 grid points in  $x$ -direction. Quantity  $1 - F \times n_0$  is the plasma minimal number density in the slab. Note that for case 3,  $F = 0.2$  and for case 4,  $F = 0.99$ , respectively. An explanation for the factor  $F$  will be given below after the EM wave driving will be specified. Number densities for the cases 3 and 4 graphically are shown in figures 3(a) and 4(a), respectively.

For the cases 5 and 6 the number density used is given by equation(8)

$$n_{e,i}(x, y) = \begin{cases} \text{if } [(x < 512/n_x x_{\text{max}}) \\ \text{or } (x > 1024/n_x x_{\text{max}}), 10^{-2}n_0, n_0] \\ \times \left( 1 - F \times \left[ e^{-(y-24/n_y y_{\text{max}})^8/L_y^8} + e^{-(y-64/n_y y_{\text{max}})^8/L_y^8} \right. \right. \\ \left. \left. + e^{-(y-104/n_y y_{\text{max}})^8/L_y^8} \right] \times e^{-(x-768/n_x x_{\text{max}})^8/L_x^8} \right), \end{cases} \quad (8)$$

where  $L_y = y_{\text{max}}/10$  and  $L_x = x_{\text{max}}/64$  are the width of density structures and  $y$ - and  $x$ -directions. Number densities for the cases 5 and 6 are plotted in figures 5(a) and 6(a), respectively. In equation (8) for case 5 we set  $F = 0.2$  and for case 6 it is set to  $F = 0.99$ , respectively. Note that 768th grid is right in the middle between 512 and 1024 grid points in  $x$ -direction. This is the interval where both plasma and metamaterial are present in the cases 5 and 6.

With number densities in all numerical runs specified, next we describe how we generate (drive) EM waves. Similar to [1] we drive  $x = 1\Delta$  cell as described in Appendix A. Here we only need to explain the driving field amplitude  $E_0 = 760199.13 \text{ V m}^{-1}$ , which produces linearly polarized in  $z$ -direction EM wave that propagates in both positive and negative  $x$ -directions. Note that because of periodic boundary conditions used, left propagating wave (i.e one that travels in the negative  $x$ -direction), re-enters the simulation domain from the right edge of the domain, as shown in figure 1(a). We also need to comment on the frequency  $\omega_0 = 1.1893397 \times 10^9 \text{ Hz}$  radian. Firstly,  $E_0$  is set to  $E_0 = 0.25\omega_{pe}m_e c/q_e = 760199.13 \text{ V m}^{-1}$ . The relevant electric field scale in this context is so called wave breaking electric field. The relevant parameter is  $a = q_e E_0/(m_e \omega_0 c)$  [28]. When  $a \geq 1$ , the electron quiver motion is relativistic and the EM-plasma interaction is non-linear (wave breaks, i.e. over-turns due to non-linearity). EM wave stays linear otherwise for  $a \leq 1$ . For our value of  $E_0$  used

$a = 0.375$ , which means our results stay in the moderately linear regime. Secondly, we set  $\omega_0 = \omega_{pe}/1.5 = 1.1893397 \times 10^9$  Hz rad. This means that EM wave cannot propagate through plasma having number density  $n_0 = 10^{15}$  particles per  $m^{-3}$ , as  $\omega_0$  is a factor of 1.5 below the plasma frequency.

We now can explain the use of  $F = 0.2$  and  $F = 0.99$  factors in equations (7) and (8) (see also table I).  $(1 - F) \times 1.5 = 1.2$  for  $F = 0.2$  and  $(1 - F) \times 1.5 = 0.015$  for  $F = 0.99$ . In the first case ( $(1 - F) \times 1.5 = 1.2$ ) plasma metamaterial composite is *transparent* to EM wave with negative phase speed propagation, while in the second case ( $(1 - F) \times 1.5 = 0.015$ ) plasma metamaterial composite is *opaque* to EM wave.

### A. Quasi 1D Results

One of the aims of this work is to extend previous one dimensional studies of EM wave propagation on an over-dense plasma-metamaterial [1] composite into two spatial dimensions. This is achieved in 4 numerical runs for cases 1a, 1b, 1c and 1d, see table I for details. The cases 1(a) to 1(d) are considered in order to validate EPOCH 2D by comparing its results with Ref. [1]. EPOCH 2D was modified as explained in Appendix A. The numerical grid is essentially one dimensional:  $n_x \times n_y = 8192 \times 3$ . This is because EPOCH 2D needs at least 3 grid points in  $y$ -direction. 8192 number of grids in  $x$ -direction was chosen so that left- and right-propagating EM waves, due to periodic boundary conditions, do not collide by the end simulation time of  $t_{end} = 100/\omega_{pe}$ . This is clearly seen in figure 1(a), where we show time-distance plot of  $E_z(x, y = y_{max}/2, t)/E_0$  when electron and ion number densities are set to  $10^{-2}n_0$ , i.e. essentially plasma is so rarefied (well below under critical density), it can be regarded as a vacuum. Figure 1(a) corresponds to case 1a. In figure 1(b) we plot the same electric field component but for the case 1b, i.e. when plasma is present, but metamaterial is not. Because plasma is overdense, EM wave with frequency  $\omega_0 = \omega_{pe}/1.5$ , cannot propagate through plasma and a standing EM wave forms. In figure 1(c) we plot the same but for the case 1c, i.e. when plasma is absent ( $n_{e,i} = 10^{-2}n_0$ ), but metamaterial is present. Because metamaterial frequency is  $\omega_m = 1.7\omega_0$ , the metamaterial  $\mu_m$  is negative so again EM wave with frequency  $\omega_0$ , cannot propagate through plasma-metamaterial region and a standing EM wave forms. In figure 1(d) we plot the same but for the case 1d, i.e. when both plasma and metamaterial are present and form a composite between grid points 512 and 1024 in  $x$ -direction. We now see that in the plasma metamaterial composite region which lies in the interval  $12.8 < x < 25.6$  EM wave with frequency  $\omega_0$  propagates with negative phase speed (and positive group speed) because effective permittivity of the plasma  $\epsilon_p$  and the effective permeability of the metamaterial  $\mu_m$  are both negative. We note that our figure 1 matches closely figure 2 from Ref.[1]. Since our simulation parameters for case 1 ( $\omega_{pe} = 1.5\omega_0$  which corresponds to  $\epsilon_p = -1.25$  and  $\omega_m = 1.7\omega_0$  which corresponds to  $\mu_m = -1.89$ ) are similar, to that of Ref.[1] hence the similarly of the time-distance plots is successfully achieved.

In conclusion, figure 1 is a successful reproduction of 1D

results of Ref.[1], but now with EPOCH 2D.

### B. 2D Results

Next, in order to study 2D effects in the subsequent runs, for the testing purposes, in case 2 now the grid size is increased in  $y$ -direction to 128. That is in case 2 everything else is the same as in case 1d, but grid size is  $n_x \times n_y = 8192 \times 128$ . In figure 2(a) we show a number density slab of plasma that lies in the intervals  $12.8 < x < 25.6$  and it is uniform in  $y$ -direction with  $0 < y < 3.2$ . We note that  $n(x, y, t = 0)/n_0$  in these intervals is close to unity, i.e.  $n(x, y, t = 0)/n_0 = 1$  – see color table of figure 2(a). In figure 2(b) we plot line profile of electric field  $E_z(x, y = y_{max}/2, t = t_{end})$  in the middle grid point in  $y$  at the final simulation time. Note the different  $x$ -range of plots used in figure 2(a) and figure 2(b). In the latter the entire simulation domain length is shown, in the former only the area around plasma-metamaterial composite is presented. The purpose of figure 2(b) is to prove that the electric field of the EM wave that goes in negative  $x$ -direction and because of periodic boundary conditions re-appears on the right-side of the domain, does not collide with EM wave that goes in positive  $x$ -direction. We consider EM wave that travels in positive  $x$ -direction as a main object of our study. The negative  $x$ -direction going wave can be regarded as a parasitic wave that cannot be avoided due to imperfect means of EM wave excitation. Essentially figure 2(b) proves that because of the absence of the left-right-travelling EM wave collision, any behaviour for  $x > 100$  can be ignored. In figure 2(c) we show time-distance plot of  $E_z(x, y = y_{max}/2, t)/E_0$ . We note that this plot is very similar (if not identical) to 1(d). This is because of the uniformness in  $y$ -direction of the number density, whether  $n_y = 3$  or 128 it makes no difference. The same conclusion follow from figure 2(c) that in the region of plasma metamaterial is present ( $12.8 < x < 25.6$ ) we witness negative phase speed (and positive group speed) EM wave propagation in an over-dense plasma. In figure 2(d) we plot  $E_z(x, y, t = t_{end})/E_0$ . The purpose of this plot is to ascertain that no  $y$ -variation is seen as the problem is uniform in  $y$ -direction. Indeed, we see from figure 2(d) that this is the case.

Cases 3 and 4 aim to study blocking of EM waves by plasma-metamaterial composite barriers. Thus, in case 3 we consider a shallow slab (a barrier) where plasma number density is dropping to  $0.8n_0$ , while in case 4, number density is dropping to  $0.015n_0$ , both in the interval between 640 and 896 grid points in  $x$ -direction. In the normalized units this is  $12.8 \times 640/512 < x < 12.8 \times 896/512$  i.e.  $16 < x < 22.4$ , which can be seen as light-green color strip in the middle of figure 3(a) and a white color strip in the middle of figure 4(a). In case 3 ( $(1 - F) \times 1.5 = 1.2$ ) plasma metamaterial composite should be transparent to EM wave with negative phase speed propagation, while in case 4 ( $(1 - F) \times 1.5 = 0.015$ ) plasma metamaterial composite should be opaque to the EM wave. That is exactly what we see in figures 3(c) and 4(c): in figure 3(c) the EM wave propagates freely though the entire plasma metamaterial composite ( $12.8 < x < 25.6$ ), while in figure 4(c) EM wave is blocked by the deep density drop  $16 < x <$

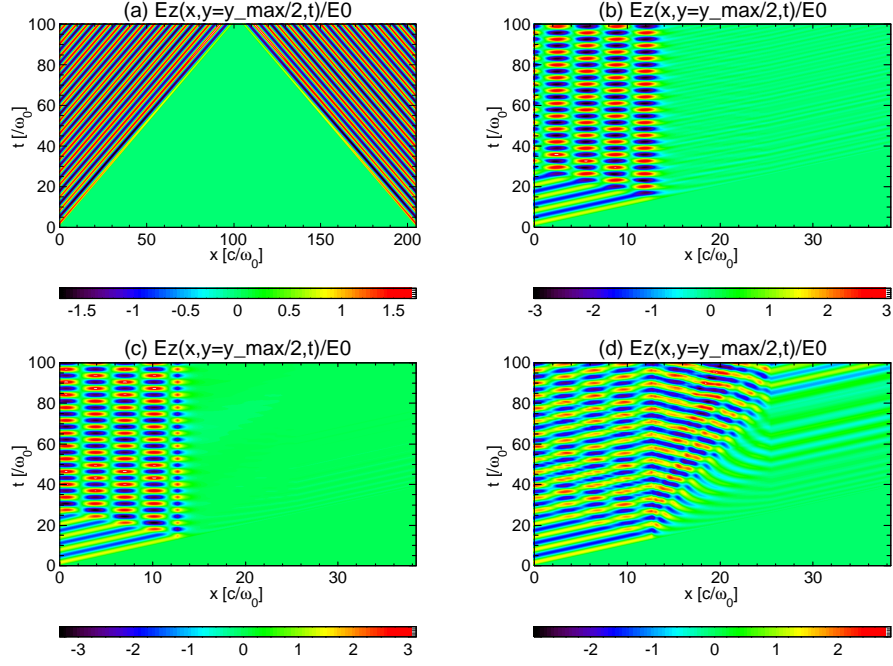


FIG. 1: Time-distance plot of  $E_z(x, y = y_{\max}/2, t)/E_0$ . (a) case 1a, (b) case 1b, (c) case 1c and (d) case 1d. See table I for details.

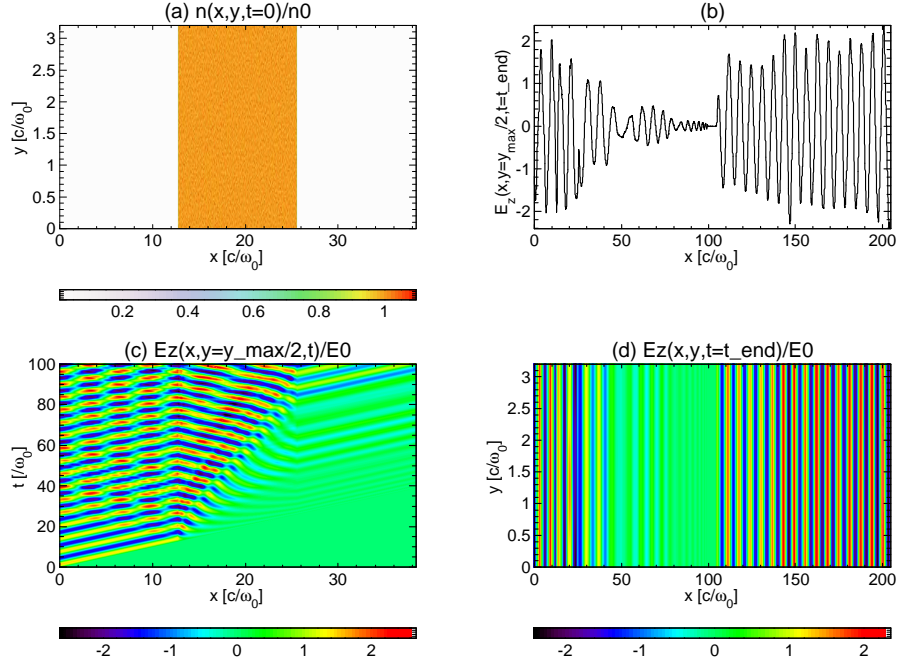


FIG. 2: Case 2: (a)  $n(x, y, t = 0)/n_0$ , (b) a line profile of  $E_z(x, y = y_{\max}/2, t = t_{\text{end}})$ , (c) time-distance plot of  $E_z(x, y = y_{\max}/2, t)/E_0$ , (d)  $E_z(x, y, t = t_{\text{end}})/E_0$ .

22.4, hence a standing EM wave forms near the  $x = 16$  edge. This way, we achieve blocking of EM wave by dropping density in the plasma metamaterial composite to an appropriate value, such that  $(1 - F) \times 1.5 < 1$  condition is met. In figure 3(b) we see similar behaviour of electric field as in 2(b), but figure 4(b)

is significantly different, we gather that  $E_z(x, y = y_{\max}/2, t = t_{\text{end}})$  amplitude is significantly reduced and the frequency of the EM wave is increased. We conjecture that only non-linear harmonics can tunnel through the density drop which acts as a barrier to negative phase speed propagation seen in figures



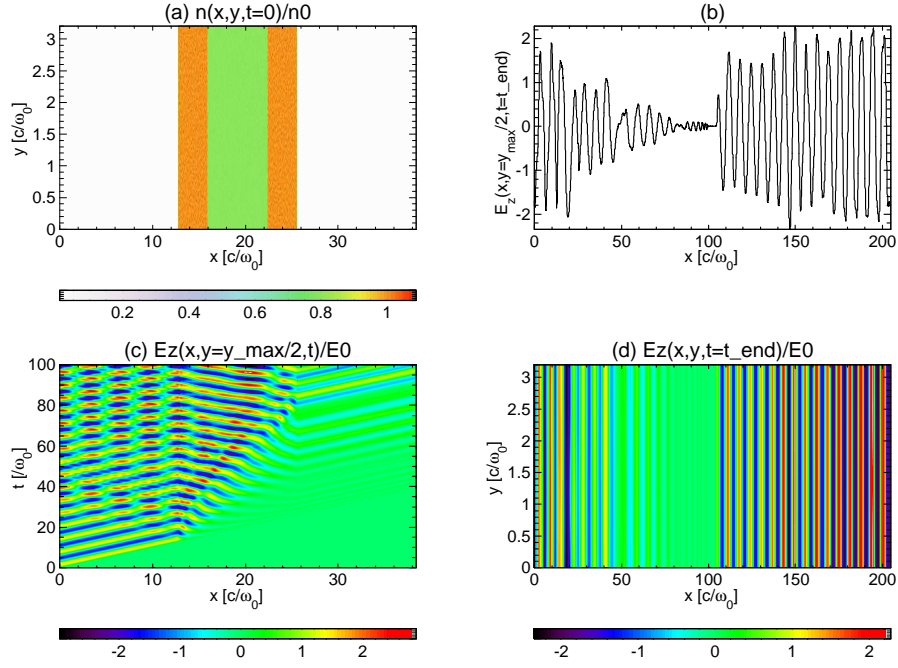


FIG. 3: The same as in figure 2, but now for case 3.

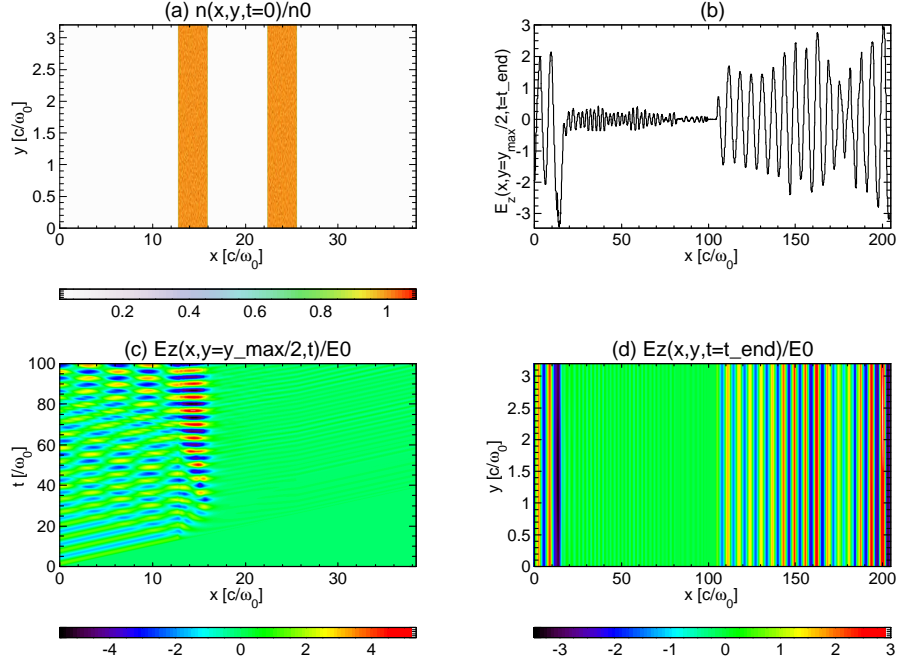


FIG. 4: The same as in figure 2, but now for case 4.

2(b,c) figure 3(b,c). For consistency we also check spatial structure of EM wave  $E_z(x, y, t = t_{\text{end}})/E_0$  in figures 3(d) and 4(d). Indeed we see in figure 4(d) that EM wave that propagates in the positive  $x$ -direction, does not move beyond  $x > 16$ , as it is effectively blocked.

Cases 5 and 6 also aim to study blocking of EM waves by plasma-metamaterial composite, but instead of a slab we con-

sider two-dimensional density rectangular depletions (DRD) that can be seen in figures 5(a) and 6(a), as light-green and white color boxes. In them, the number density drops to  $0.8n_0$  in case 5 (as in case 3) and  $0.015n_0$  in case 6 (as in case 4). Their dimensions are  $x_{\text{rect}} = 22 - 16 = 6$  and  $y_{\text{rect}} = 0.64 \approx 1$  i.e.  $y_{\text{rect}} \approx c/\omega_0$ . The gaps between DRDs are 0.32, i.e.  $\approx (1/3) \times (c/\omega_0)$ . Essentially, we wanted to add some struc-

turing in  $y$ -direction with structures on the scale of EM wave inertial length of  $\approx c/\omega_0$ . The results of the last two entries from table I are shown in figures 5 and 6. We gather from figures 5 and 6 that shallow DRDs are transparent to EM wave, while deep ones block EM wave, as expected. Next, we focus our attention on the differences from cases 3 and 4, presented earlier in figures 3 and 4. It can be seen in figure 6(b) that electric field from has complex beating pattern (multiple harmonic beating). This is in contrast to figure 4(b) where high frequency harmonics show a regular spatial pattern (no beats). Figure 6(d) does not show any structuring in  $y$ -direction, which seems somewhat counter intuitive. As, for example, it seems not clear at first sight, why in-between DRDs across  $y$ -coordinate where normalized plasma number density is unity, i.e. in the four light-brown color strips on top and bottom of white rectangles in figure 6(a), no clear EM wave propagation seen. Our explanation is that shortness of the considered gaps,  $\approx (1/3) \times (c/\omega_0)$ , is not sufficient for apparent EM wave front propagation as the wave interacts with plasma on circa  $> c/\omega_0$  scale. Nonetheless, the beats are seen in 6(b), which means there is some propagation in the gaps, hence the beat pattern. Ideally, in retrospect, we surmise that a bigger than  $n_y = 128$  could have been considered. Nonetheless, we still think the considered  $y$ -coordinate structuring in cases 5 and 6 provide a useful information. Future, a more elaborate study, could potentially consider different shapes of DRDs and different separation distances, which could be a subject to next work(s).

In conclusion, here we established that plasma-metamaterial composite can block EM waves by both slab and DRD configurations. This happens by forming a standing wave that subsequently damps at the edge of an opaque region.

#### IV. CONCLUSIONS

The aim of this work is two-fold: (i) to extend previous 1D studies [1] of electromagnetic (EM) waves propagation in an over-dense plasma-metamaterial composite into 2D spatial dimensions and (ii) to study blocking of EM waves by the composite 2D structures that act like barriers, which is analogous to EM wave trapping by preformed density cavities in near-critical density plasmas [26]. Our study comprises of several logical steps:

1. In Appendix A we presented a numerical recipe how to include the presence of metamaterial in plasma by adding additional current  $J_m$  using EPOCH 2D PIC code.
2. We then validated the modification of EPOCH code (figure 1, cases 1a, 1b, 1c and 1d, see table I) by a successful reproduction of 1D results of Ref.[1] with EPOCH 2D on a  $n_x \times n_y = 8192 \times 3$  grid.
3. With a purpose to study 2D effects in this work, in case 2 we increased grid size  $y$ -direction to 128 and ascertained negative phase speed propagation (figure 2(c)) which is nearly identical to figure 1(d) (the quasi-1D case with  $n_y = 3$  grids along  $y$ -axis).
4. Next, we wanted to study EM wave blocking by a slab of density depletion (cases 3 and 4). Thus, we set plasma num-

ber density according to equation (7). We find that in case 3  $((1 - F) \times 1.5 = 1.2)$  plasma metamaterial composite is transparent to EM wave. In this case EM wave propagates with a negative phase speed, while in case 4  $((1 - F) \times 1.5 = 0.015)$  plasma metamaterial composite is opaque to the EM wave. Thus, forming a standing wave at the edge of an opaque region. Here the generic conclusions are as following: (i) if  $(1 - F) \times n_0$  is the minimal number density of the plasma slab and (ii)  $f = \omega_{pe}/\omega_0$  is the factor by which EM wave's angular frequency  $\omega_0$  is less than electron plasma frequency  $\omega_{pe}$ , then the condition for EM wave blocking by the slab is

$$(1 - F) \times f < 1. \quad (9)$$

We also find that when condition given by equation (9) is met, EM amplitude is significantly reduced and the frequency of the EM wave is increased (figure 4(b)). This leads to a conclusion that only non-linear harmonics can tunnel through the density drop which acts as a barrier to negative phase speed propagation found in figures 2(b,c) figure 3(b,c).

5. Further, we aimed to study EM wave blocking by two-dimensional DRDs (cases 5 and 6). Therefore plasma number density was set according to equation (8). We find that for the sizes and shapes of DRDs considered, behaviour is similar to the plasma slab density depletion. The main difference is that electric field from. It now has complex beating pattern (figure 6(b)). Such behaviour is in contrast to figure 4(b), where where high frequency harmonics show a regular spatial pattern and no beats are present. For two-dimensional DRDs the EM wave blocking condition is also given by equation (9).

In summary, the barriers for EM wave propagation are created when metamaterial spatially co-exists with a plasma density depletion in a form of a slab or two-dimensional DRDs. Such approach is analogous to EM wave trapping by preformed density cavities in near-critical density plasmas investigated by Ref. [26]. We have shown that plasma metamaterial composite allows to block EM waves by both a slab (figure 4(c)) and DRD configurations (figure 6(c)). In both cases a standing wave at the edge of an opaque region is formed. The EM wave blocking condition is established by equation (9), which is supported by our PIC numerical simulations. In our approach metamaterial *acts like an agent that lets EM wave to enter over-dense plasma*. The subsequent density drop *makes plasma opaque to the EM wave*, effectively blocking it in form of a standing wave at the edge of the barrier (density depletion slab or two dimensional DRDs).

Ref. [26] established that in a situation when a near-critical density plasma contains a preformed density cavity, EM wave is trapped and becomes a standing wave. Their 2D PIC simulations have shown that within  $100 - 200/\omega_0$  the standing wave damps away. We only show numerical results with end simulation time of  $100/\omega_0$ , but confirm similar result to Ref. [26] that within few hundred  $1/\omega_0$  EM wave indeed damps. We suggest that the wave damping can offer applications such as heat deposition or substrate materials (micro)machining [29] depending on EM wave intensity. Low intensity EM waves would simply heat the plasma, potentially, high intensity EM waves can be used for substrate materials (micro)machining. From figure 4(c) (density depletion slab case) and figure 6(c)



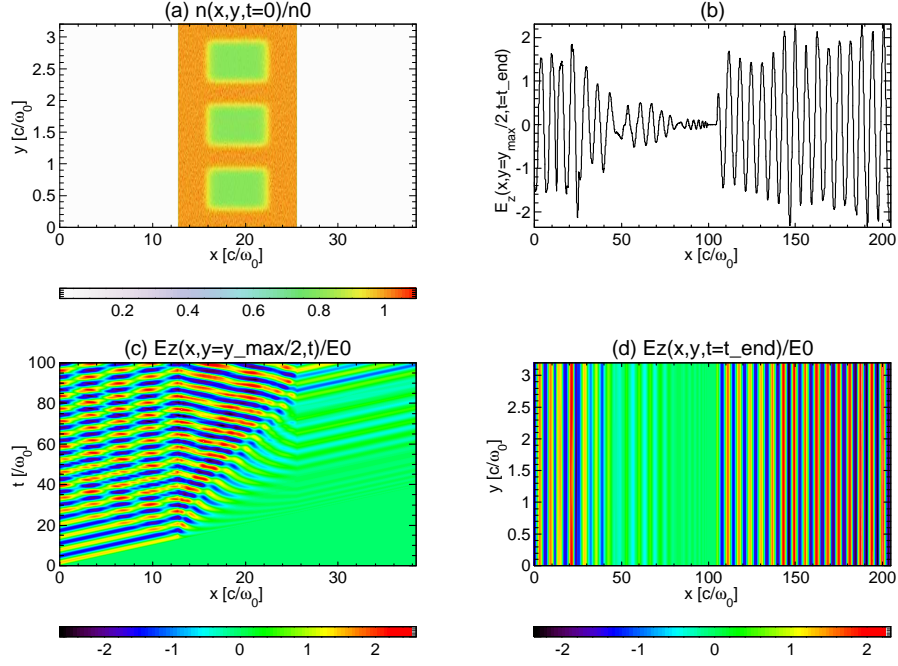


FIG. 5: The same as in figure 2, but now for case 5.

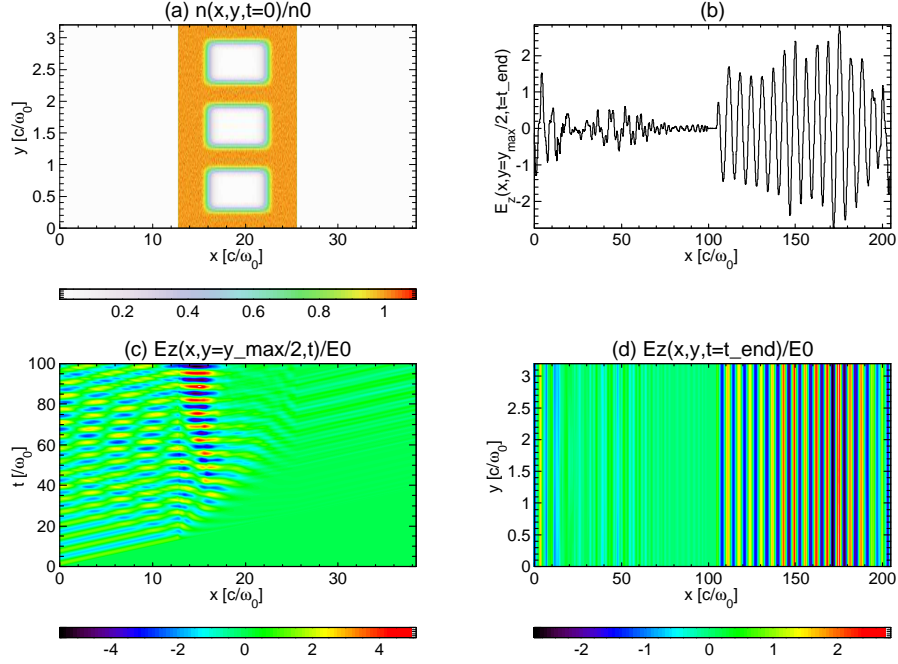


FIG. 6: The same as in figure 2, but now for case 6.

(two-dimensional DRDs case) we see that length scale of the standing wave pattern is  $(1 - 2)c/\omega_0 = 0.25 - 0.5$  m. Obviously this is the value for  $n_0 = 10^{15}$  particles per  $\text{m}^{-3}$  used, because number density sets  $\omega_{pe} = 1.784 \times 10^9$  Hz rad, which, in turn, sets  $\omega_0 = \omega_{pe}/1.5 = 1.189 \times 10^9$  Hz rad. Setting higher number density say  $n_0 = 10^{19} \text{ m}^{-3}$ , can make  $c/\omega_0$  as small as 2.5 mm.

We would like to stress the difference in approach by Luan *et al.* [26] and this work. In particular, Luan *et al.* [26] consider situation when the strength of the electric field is high enough, electron density increases such that EM waves tends to be reflected by the plasma layer. Hence, in that case, the plasma is first allowing propagation of high-power EM pulse, and then blocking it as a function of time when electron den-

sity increases. In our case, the background number density does not change markedly as the time progresses. We do not keep it artificially static, it slowly evolves in time as PIC simulation progresses. Thus our a potential applications are different from that of Luan *et al.* [26]. Our results potentially suggest yet unexplored and/or unknown applications of controlling EM waves with plasma and metamaterial composite. These may include: a more efficient PVD (because the reaction rate is proportional to the product of number densities of the reactant species), controlling EM wave propagation (EM wave blocking) in invisibility cloaks and perhaps something yet to be discovered in the future.

We would like to remark that kinetic PIC electromagnetic simulations are more realistic than fluid FDTD simulations to capture the nonlinear effects in the plasma due to incident high-power EM energy. In this paper, we only consider low-power cases ( $a = 0.375$ ) where the physics remains linear. It should be interesting to study novel features provided by PIC simulations in the *nonlinear* case, for instance by showing the electron energy distribution modifications such as in Iwai *et al.* [1]. This will be subject of a subsequent work.

In the future, it would be also interesting to explore the novelties brought about by the 2D model, by studying, for example, the effect of *the angle of incidence* of the EM wave on the composite of plasma and metamaterial slab.

Yet another future avenue of research could be developing an analytical model to validate the numerical results. Indeed, air can be modeled as a propagating *transmission line*, while plasma as an evanescent one, and finally the combination of plasma with MNG material as a propagating transmission line. It would be feasible to analytically calculate their characteristic (i.e., intrinsic) impedance and propagation constant. The valuable end-product of such an analytical calculation could be reflection and transmission coefficients of the complex structure so that numerical results can be validated by such a model. Another possibility for an analytical model is to consider so-called Zakharov's equations in order to describe the electronic plasma waves. In such model the slowly varying envelope of the electric field is coupled to the low-frequency variation of the density of the ions. Colin and Colin [30] used it in a situation when the laser enters the plasma, then part of it is backscattered through a Raman-type process and a Brillouin-type process. The Raman and Brillouin parts and the laser combine together to create an electron-plasma wave. These four waves interact in order to create a low-frequency variation of density of the ions which has itself an influence on the four preceding waves.

There are many examples when there is a good reason to conduct multi-scale numerical simulations combining ab initio/density functional theory/molecular dynamics-type simulations [31] and meso-scale, particle-in-cell-based modelling, such as: (i) correlated simulation studies concerning plasma charging and its effects over ten orders of magnitude in length scales at the lunar terminator [32], (ii) dynamic coupling between particle-in-cell and atomistic simulations to simulate metal surface response to high electric fields [33], (iii) molecular dynamics model and particle-in-cell model to investigate the physics of ionic electrospray propulsion over 9 orders of

magnitude in length scale [34], (iv) multi-scale/hybrid modelling of low temperature plasmas for fundamental investigations and equipment design [35], (v) gas discharge plasmas used for various materials science applications [36]. Future extensions of this work will be combining molecular dynamics and particle-in-cell modeling as e.g. in Ref.[33].

An interesting observation can be also made as follows: When the de-Broglie wavelength of plasma particles becomes of the order of mean inter-particle distance, quantum effects such as the combined effect of Bohm potential and exchange correlation potential significantly modifies the dispersion properties of e.g. lower hybrid wave [37]. In the case when plasma density is high the exchange correlation potential can in principle dominate over the particle dispersion effects [38–40]. Broadly speaking this exchange correlation potential can be regarded as a form of the density fluctuation theory (DFT) [38]. The influence of exchange potential and Bohm force on the propagation characteristics of different type of waves in plasmas have been investigated before [38–40]. Since the number densities considered here, in principle, are high enough to invoke the quantum effects such as (i) the exchange correlation potential, (ii) Bohm potential, any future works on the subject should consider incorporating these for completeness.

## ACKNOWLEDGEMENTS

The author would like to thank: (i) The two anonymous referees for useful comments that improved this manuscript and (ii) The Senior Editor Dr Francesco Taccogna for organizing useful and rigorous review process.

**Data availability statement.** The data and numerical codes that support the findings of this study are available from the corresponding author upon reasonable request.

## Appendix A: Appendixes

Here we present a numerical recipe how to include the presence of metamaterial in plasma by adding the additional current  $J_m$  using EPOCH PIC code [21]. The latter can be downloaded from GitHub repository <https://epochpic.github.io/quickstart.html>.

Step 1: edit `src/epoch2d.F90` and after line

```
CALL open_files      ! setup.f90
```

initialize  $J_{m,y}$  as zero value

```
jmy(:,:) = 0.0_num.
```

Note that "underscore num" is making sure that EPOCH is using F90 double precision, which is EPOCH's default accuracy. Historically using the compiler auto-promotion of REAL to DOUBLE PRECISION was unreliable, so EPOCH uses "kind" tags to specify the precision of the code. See section 1.5 in the EPOCH user manual.

Step 2: edit

src/shared\_data.F90

and in the following line add  $J_{m,y}$  declaration (last entry):

```
REAL(num), ALLOCATABLE, DIMENSION(:, :) :: &
ex, ey, ez, bx, by, bz, jx, jy, jz, jmy
```

Step 3: edit

src/housekeeping/mpi\_routines.F90

and after line 388 add

```
ALLOCATE(jmy(1-jng:nx+jng, 1-jng:ny+jng))
```

to allocate  $J_{m,y}$  array.

Step 4: edit src/fields.f90 and after line "CONTAINS" add two following subroutines in the case of both plasma and metamaterial composite are present. If metamaterial is absent and only electric field of EM wave needs to be driven, then only leave the 1st subroutine. Below are the said two subroutines:

```
SUBROUTINE drive_field(time)
REAL(num), INTENT(IN) :: time
IF (x_min_boundary) THEN
  ez(1,:) = ez(1,:) + 760199.13_num*&
  sin(1.1893397e+09_num*time)
END IF
END SUBROUTINE drive_field

SUBROUTINE drive_mfield(time)
REAL(num), INTENT(IN) :: time
IF (x_min_boundary) THEN
  jmy(512:1024,:) = jmy(512:1024,:) + hdt*&
  (1.7_num*1.1893397e+09_num)**2*by(512:1024,:)
```

```
by(512:1024,:) = by(512:1024,:) - &
hdt*jmy(512:1024,:)
END IF
END SUBROUTINE drive_mfield
```

Further, in the end of src/fields.f90 file, after half-time step and full time step the following calls to the said routines should be added:

```
CALL update_e_field
CALL drive_field(time+0.5_num*dt)
CALL efield_bcs
CALL update_b_field
CALL drive_mfield(time+0.5_num*dt)
...
CALL update_b_field
CALL drive_mfield(time+dt)
CALL bfield_final_bcs
CALL update_e_field
CALL drive_field(time+dt)
CALL efield_bcs
```

Note that there is no need to modify EM solver part in the src/fields.f90 file. The fact that presence of metamaterial is implemented by setting  $J_m$  as in the above subroutine `jmy(512 : 1024, :)` puts a *restriction* on number of processors that can be used in  $x$ -direction. The grid cells 512 : 1024 must fit on the first processor. Thus, because  $8192/1024 = 8$ , we are restricted to use no more than 8 processors in  $x$ -direction. There is no restriction on number of processors in  $y$ -direction. EPOCH code allows simulation domain decomposition to be set manually. In this work we have used EPOCH's `nprocx=8` and `nprocy=1` setting.

- 
- [1] A. Iwai, O. Sakai, and Y. Omura, *Physics of Plasmas* **24**, 122112 (2017).
  - [2] M. A. Lieberman and A. J. Lichtenberg, *Principles of Plasma Discharges and Materials Processing* (Wiley, Hoboken, 1994).
  - [3] H. Sugai, I. Ghanashev, and M. Nagatsu, *Plasma Sources Science and Technology* **7**, 192 (1998).
  - [4] V. G. Veselago, *Soviet Physics Uspekhi* **10**, 509 (1968).
  - [5] J. Pendry, A. Holden, D. Robbins, and W. Stewart, *IEEE Transactions on Microwave Theory and Techniques* **47**, 2075 (1999).
  - [6] R. W. Ziolkowski and E. Heyman, *Phys. Rev. E* **64**, 056625 (2001).
  - [7] S. Foteinopoulou, E. N. Economou, and C. M. Soukoulis, *Phys. Rev. Lett.* **90**, 107402 (2003).
  - [8] V. M. Agranovich, Y. R. Shen, R. H. Baughman, and A. A. Zakhidov, *Phys. Rev. B* **69**, 165112 (2004).
  - [9] I. V. Shadrivov, A. A. Zharov, and Y. S. Kivshar, *J. Opt. Soc. Am. B* **23**, 529 (2006).
  - [10] R. Boyd, *Nonlinear Optics, 3rd ed.* (Elsevier, London, 2008).
  - [11] R. A. Shelby, D. R. Smith, and S. Schultz, *Science* **292**, 77 (2001).
  - [12] A. A. Houck, J. B. Brock, and I. L. Chuang, *Phys. Rev. Lett.* **90**, 137401 (2003).
  - [13] C. G. Parazzoli, R. B. Greegor, K. Li, B. E. C. Koltenbah, and M. Tanielian, *Phys. Rev. Lett.* **90**, 107401 (2003).
  - [14] W. Rotman, *IRE Transactions on Antennas and Propagation* **10**, 82 (1962).
  - [15] Y. Nakamura and O. Sakai, *Japanese Journal of Applied Physics* **53**, 03DB04 (2014).
  - [16] A. Iwai, Y. Nakamura, A. Bambina, and O. Sakai, *Applied Physics Express* **8**, 056201 (2015).
  - [17] A. Iwai, Y. Nakamura, and O. Sakai, *Phys. Rev. E* **92**, 033105 (2015).
  - [18] O. Sakai, *Journal of Applied Physics* **109**, 084914 (2011).
  - [19] K. Kourtzanidis, D. M. Pederson, and L. L. Raja, *Journal of Applied Physics* **119**, 204904 (2016).
  - [20] A. Iwai, Y. Nakamura, O. Sakai, and Y. Omura, *Plasma Sources Science and Technology* **29**, 035012 (2020).
  - [21] T. D. Arber, K. Bennett, C. S. Brady, A. Lawrence-Douglas, M. G. Ramsay, N. J. Sircombe, P. Gillies, R. G. Evans, H. Schmitz, A. R. Bell, and C. P. Ridgers, *Plasma Physics and Controlled Fusion* **57**, 113001 (2015).
  - [22] M. Y. Yu, P. K. Shukla, and K. H. Spatschek, *Phys. Rev. A* **18**, 1591 (1978).
  - [23] X. Wang, W. Yu, M. Y. Yu, H. Xu, J. W. Wang, and X. Yuan, *Physics of Plasmas* **16**, 053107 (2009).
  - [24] S. Luan, W. Yu, W. Xu, M. Murakami, H. Zhuo, J. Wang,

- X. Wang, and H. Wu, Applied Physics B **108**, 875 (2012).
- [25] B. Zhu, Y.-C. Wu, K.-G. Dong, W. Hong, J. Teng, W.-M. Zhou, L.-F. Cao, and Y.-Q. Gu, Physics of Plasmas **19**, 102304 (2012).
- [26] S. Luan, W. Yu, J. Wang, M. Yu, S. Weng, M. Murakami, J. Wang, H. Xu, and H. Zhuo, Laser and Particle Beams **31**, 589 (2013).
- [27] D. Tsiklauri, Research in Astronomy and Astrophysics **24**, 095021 (2024).
- [28] E. Esarey, C. B. Schroeder, and W. P. Leemans, Rev. Mod. Phys. **81**, 1229 (2009).
- [29] B. Stockdale, JALA: Journal of the Association for Laboratory Automation **4**, 35 (1999).
- [30] M. Colin and T. Colin, Differential and Integral Equations **17** (2004).
- [31] S. Jenkins and I. Morrison, Chemical Physics Letters **317**, 97 (2000).
- [32] J. Wang and Z. Huang, IEEE Transactions on Plasma Science **51**, 2561 (2023).
- [33] M. Veske, A. Kyritsakis, F. Djurabekova, K. N. Sjobak, A. Aabloo, and V. Zadin, Phys. Rev. E **101**, 053307 (2020).
- [34] J. Asher, Z. Huang, C. Cui, and J. Wang, Journal of Applied Physics **131**, 014902 (2022).
- [35] M. J. Kushner, Journal of Physics D: Applied Physics **42**, 194013 (2009).
- [36] A. Bogaerts, K. De Bleecker, V. Georgieva, I. Kolev, M. Madani, and E. Neyts, Plasma Processes and Polymers **3**, 110 (2006).
- [37] T. Rimza and P. Sharma, Journal of Physics: Conference Series **836**, 012028 (2017).
- [38] R. Maroof, A. Mushtaq, and A. Qamar, Physics of Plasmas **23**, 013704 (2016).
- [39] M. Jamil, A. Rasheed, C. Rozina, Y.-D. Jung, and M. Salimullah, Physics of Plasmas **22**, 082113 (2015).
- [40] M. Shahmansouri and A. P. Misra, Physics of Plasmas **23**, 072105 (2016).
- [41] N. Selvakumar and H. C. Barshilia, Solar Energy Materials and Solar Cells **98**, 1 (2012).
- [42] J. Hanlon and R. J. Kelsey, *Handbook of Package Engineering* (CRC Press, Boca Raton, 1998).
- [43] E. Fortunato, P. Barquinha, and R. Martins, Advanced Materials **24**, 2945 (2012).